

Non-monotonic Casimir interaction: The role of amplifying dielectrics

Morteza Soltani,¹ Jalal Sarabadani,^{2,*} and S. Peyman Zakeri¹

¹*Department of Physics, University of Isfahan, Isfahan 81746, Iran*

²*Department of Applied Physics, and COMP Center of Excellence, Aalto University School of Science, P.O. Box 11000, FI-00076 Aalto, Espoo, Finland*

The normal and the lateral Casimir interactions between corrugated ideal metallic plates in the presence of an amplifying or an absorptive dielectric slab has been studied by the path-integral quantization technique. The effect of the amplifying slab, which is located between corrugated conductors, is to increase the normal and lateral Casimir interactions, while the presence of the absorptive slab diminishes the interactions. These effects are more pronounced if the thickness of the slab increases, and also if the slab comes closer to one of the bounding conductors. When both bounding ideal conductors are flat, the normal Casimir force is non-monotonic in the presence of the amplifying slab and the system has a stable mechanical equilibrium state, while the force is attractive and is weakened by intervening the absorptive dielectric slab in the cavity. By replacing one of the flat conductors by a flat ideal permeable plate the force becomes non-monotonic and the system has an unstable mechanical equilibrium state in the presence of either an amplifying or an absorptive slab. When the left side plate is conductor and the right one is permeable, the force is non-monotonic in the presence of a double-layer DA (dissipative-amplifying) dielectric slab with a stable mechanical equilibrium state, while it is purely repulsive in the presence of a double-layer AD (amplifying-dissipative) dielectric slab.

PACS numbers: 42.50.Lc, 03.70.+k, 42.50.-p

I. INTRODUCTION

An interesting macroscopic result of confinement of the quantum electromagnetic (EM) field between two ideal parallel flat conductors is the Casimir effect [1]. Comparing the energy of the system in the presence and in the absence of bounding ideal metallic plates leads to a finite attractive potential energy. The derivation of this finite energy with respect to the distance between two plates, H , is the Casimir force, F_C . The Casimir force per unit area, S , is then read as $\frac{F_C}{S} = -\frac{\hbar c \pi^2}{240 H^4}$, where \hbar is the Planck constant multiplied by $\frac{1}{2\pi}$, and c is the speed of light in the vacuum [2]. The magnitude of this force is significant when H is less than a micron [3]. Therefore the Casimir effect must be taken into account in designing micro- and nano-devices [4–7].

In addition to the normal Casimir force, corrugated conductors can experience lateral Casimir force due to the translational symmetry breaking which has been observed experimentally in 2002 [8]. The lateral Casimir effect between two rough conductors with sinusoidal corrugation has been studied theoretically in the context of path-integral formalism [9–11]. This force is very sensitive to the characteristics of the rough surfaces and also sensitive to the medium in between them. For a system composed of two rough ideal conductors immersed in the quantum vacuum, at fixed mean separation distance between two conductors, H , with λ as the wavelength of corrugations on both plates, the stable and unstable equilibrium states for the position of the rough plates in the

lateral direction occur when $l = (n + \frac{1}{2})\lambda$ and $l = n\lambda$, respectively [10], whereas for the system composed of a rough ideal conductor and an infinitely permeable corrugated plate, with the same H and λ , the stable and unstable equilibrium states for the position of the plates in the lateral direction occur when $l = n\lambda$ and $l = (n + \frac{1}{2})\lambda$, respectively [12].

Moreover, the Casimir force also strongly depends on

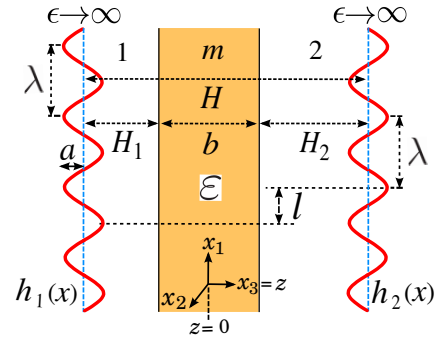


FIG. 1. (Color online) The schematic figure of a dielectric slab with dielectric function ϵ and thickness b immersed in the quantum vacuum and enclosed by two rough metallic plates. The mean distance between two plates is H . The corrugation amplitude and wavelength for both plates are a and λ , respectively. The mean distance between the left metallic plate and the left side of the dielectric slab is H_1 , while the mean distance between the right metallic plate and the right side of the dielectric slab is H_2 . The lateral mismatch between metallic plates is l . The corrugations on the left and on the right conductors are given by two height functions $h_1(x)$ and $h_2(x)$, respectively. The regions labeled by 1 and 2 are filled by the quantum vacuum while the dielectric slab is labeled by m .

* jalal.sarabadani@aalto.fi

the characteristics of the medium between the bounding plates. In a series of papers, it has been shown that the presence of absorptive dielectric medium between two bounding conductors can weaken the normal and lateral Casimir interactions [13–16]. The reason is that the absorptive dielectrics can dissipate the EM energy [17–19]. In the other hand, it has been shown that if the energy is pumped into the medium artificially, for example by lasers, the EM energy can be amplified in some regions of frequency [20–24]. These kinds of media are called *amplifying* media, where the EM energy can be amplified. Although the physical properties of these media are different from those of dissipative dielectrics, the same formal methods can be used to quantize the EM field in the presence of amplifying dielectrics as of dissipative dielectrics [20, 21, 24].

To study an amplifying medium, one can introduce a susceptibility which must satisfy the Kramers-Kronig relations. Similar to the dissipative (or absorptive) dielectrics, the dielectric function of an amplifying medium, that is $\varepsilon_{\text{amp}}(\omega)$, should have an imaginary part. But for dissipative dielectrics, the imaginary part of the dielectric function is positive, i.e. $\varepsilon_{\text{I,disp}}(\omega) > 0$, whereas for amplifying media, the imaginary part is negative, i.e. $\varepsilon_{\text{I,amp}}(\omega) < 0$ [21]. The same is true for the imaginary parts of the permeability of the dissipative and amplifying media [23]. One can quantize the EM field in the presence of the amplifying medium by adding a noise term into Maxwell equations [21, 24, 25], or using the canonical approach [21]. For quantization of the EM field in the presence of an amplifying medium, we use the path-integral formalism [13]. It should be noted that although the methods for field quantization which we use here for the amplifying and dissipative systems are the same, however the characteristics of these two kinds of systems are completely different. For example, vacuum fluctuations in the presence of dissipative and amplifying media behave in different ways. Moreover, an amplifying medium can be used to compensate the effect of dissipation [21].

In the present paper, we study and compare the normal and the lateral Casimir interactions between two rough ideal conductors in the presence of an intervening dissipative or amplifying slab, or a double-layer with mixture of them. This paper is organized as follows: In Sec. II we generally introduce the path-integral formalism to obtain the Casimir interaction energy for the system composed of a dielectric slab between two ideal rough metallic plates. Section III is devoted to study the Casimir interaction in a system composed of either an absorptive or an amplifying slab or a double-layer dielectric slab between two flat bounding ideal plates. In Sec. IV we calculate and compare the normal and the lateral Casimir interactions due to the corrugation on the bounding plates in the presence of either an absorptive or an amplifying slab. Finally we wrap up the paper with a conclusion in Sec. V.

II. FORMALISM

A. Quantization of the EM field

In this section we investigate the Casimir interaction between two ideal corrugated conductive plates in the presence of either a dissipative or an amplifying slab as depicted in Fig.1. $X = (x_0, \mathbf{x})$ is the coordinate of a point in four-dimensional time-space with the temporal coordinate x_0 , and the spatial coordinates $\mathbf{x} = (x_1, x_2, x_3)$, $x = (x_1, x_2)$. z component of X_1 , which is in the direction of x_3 , on the left conductor is $z = -H_1 - b/2 + h_1(x)$, while z component of X_2 on the right conductor is $z = H_2 + b/2 + h_2(x)$, where $h_1(x)$ and $h_2(x)$ are the deformation fields on the left and on the right ideal plates, respectively. The average distance between two conductors is H , the corrugation amplitude for both conductors is a , the wave length of the corrugation in x_1 direction for both conductors is λ , l is the lateral shift between surfaces in x_1 direction, H_1 is the mean distance of the left side of the slab and the left conductor, H_2 is the mean distance of the right side of the slab and the right conductor, and b is the thickness of the slab.

To study the Casimir interaction between two corrugated ideal metallic plates in the presence of an intervening dissipative or amplifying slab (see Fig.1), we first use the path-integral method to quantize the EM field. As we are only considering a uni-axial cavity, therefore the EM field can be decomposed into the transverse magnetic (TM) and transverse electric (TE) waves which satisfy Dirichlet (D) and Neumann (N) boundary conditions (BCs), respectively on both plates [10, 11, 26]. The D BC should be satisfied by TM waves, that is $\phi(X_a) = 0$, on both plates, while TE waves satisfy the N BC, that is $\partial_n \phi(X_a) = 0$, where $a = 1, 2$ determines the left and right plates, respectively. Consequently, after decomposing the EM field into TM and TE waves we quantize a massless scalar Klein-Gordon field, ϕ , in the presence of a dielectric slab between two conducting plates. To this end, we use the same method as of Refs.[13–16]. The dielectric medium can be a dissipative dielectric slab with a positive imaginary part of its dielectric function, that is $\varepsilon_{\text{I,disp}}(\omega) > 0$, or it can be an amplifying slab with a negative imaginary part of its dielectric function in some frequency ranges, that is $\varepsilon_{\text{I,amp}}(\omega) < 0$. The dielectric medium can be a layered dielectrics with mixture of dissipative and amplifying layers. Here, for the sake of simplicity and brevity we just present the formalism for a slab with only one dielectric layer, that can be either an absorptive or an amplifying, in between the bounding conductors. To extend the path-integral formalism to study the Casimir effect in the presence of an absorptive [13] or an amplifying medium [27], one must write the Lagrangian of the system with appropriate terms that leads to the correct equations of motion. To this end, we consider the following Lagrangian density

$$\mathcal{L} = \mathcal{L}_{\text{sys}} + \mathcal{L}_{\text{mat}} + \mathcal{L}_{\text{int}}, \quad (1)$$

where $\mathcal{L}_{\text{sys}} = \frac{1}{2}\partial^\alpha\phi(X)\partial_\alpha\phi(X)$ is the Lagrangian density of Klein-Gordon field, the summation over $\alpha = x_0, x_1, x_2$ and x_3 is assumed, and as explained in the above, $X = (x_0, \mathbf{x})$ is a coordinates of a point in four-dimensional time-space. $\mathcal{L}_{\text{mat}} = \int_0^\infty d\omega \text{sgn}[\varepsilon_1(\omega)](\frac{1}{2}\dot{Y}_\omega^2 - \frac{1}{2}\omega^2 Y_\omega^2)$ is Lagrangian density of a matter field, where the matter is modeled by a continuum oscillator's field Y_ω [28], $\varepsilon_1(\omega)$ is the imaginary part of the dielectric function, and $\mathcal{L}_{\text{int}} = \phi\dot{P}$ is the interaction Lagrangian density between matter and scalar fields. $P = \int d\omega\nu(\omega)Y_\omega$ is the polarization of the medium, and $\nu(\omega)$ is the coupling function between the scalar and the matter fields [13].

Using the Lagrangian in Eq. (1), the conjugate of the canonical momentum can be found. By employing the equal time commutation relations, one can quantize the field and obtain the Hamiltonian of the system, and show that the scalar field ϕ satisfies the following equation

$$(\nabla^2 - \varepsilon(\omega)\omega^2)\phi^+(\omega) = j_N^+(r, \omega). \quad (2)$$

The positive frequency part of the current density operator, $j_N^+(r, \omega)$, is

$$j_N^+(r, \omega) = \Theta[\varepsilon_1(\omega)]\sqrt{\frac{2\omega\varepsilon_0|\varepsilon_1(\omega)|}{\pi}}\hat{a}_N(r, \omega) + \Theta[-\varepsilon_1(\omega)]\sqrt{\frac{2\omega\varepsilon_0|\varepsilon_1(\omega)|}{\pi}}\hat{a}_N^\dagger(r, \omega), \quad (3)$$

where $\Theta(\dots)$ is the Heaviside step function, \hat{a} is a bosonic field with bosonic commutation relation, and \hat{a}^\dagger is the complex transpose of \hat{a} . Then, the Hamiltonian can be written as

$$H = \int d\omega \int d^3r \sin[\varepsilon_1(\omega)]\hbar\omega\hat{a}_N^\dagger(r, \omega)\hat{a}_N(r, \omega), \quad (4)$$

where $\varepsilon_1(\omega) = 1 + \int d\omega' \frac{\text{sgn}[\varepsilon_1(\omega')]\nu^2(\omega')}{\omega^2 - \omega'^2 + i0^+}$ leads to $\nu^2(\omega) = \text{sgn}[\varepsilon_1(\omega)]\text{Im}[\varepsilon_1(\omega)]$. The main difference between the calculations for the amplifying medium and dissipative one is the presence of $\Theta[\varepsilon_1(\omega)]$ and $\text{sgn}[\varepsilon_1(\omega)]$ in the above equations that have been discussed extensively in [21, 22, 24, 25]. It should be mentioned that the Hamiltonian in Eq. (4) is consistent with the result of Ref. [24].

To quantize the field, we calculate the generating function for the interacting system [29]. The generating function is defined as

$$\begin{aligned} \mathcal{Z}[J_\phi, J_P] &= Z_0^{-1} e^{i \int dY \mathcal{L}_{\text{int}}[\frac{\delta}{\delta J_\phi(Y)}, \frac{\delta}{\delta J_P(Y)}]} \mathcal{Z}_0[J_\phi, J_\omega] \\ &= Z_0^{-1} \sum_{n=0}^{\infty} \frac{1}{n!} \left[i \int dY \frac{\delta}{\delta J_\phi(Y)} \frac{\partial}{\partial y_0} \frac{\delta}{\delta J_P(Y)} \right]^n \\ &\quad \times \mathcal{Z}_0[J_\phi, J_\omega], \end{aligned} \quad (5)$$

where $Z_0 = \int \mathcal{D}[\phi] \exp(i \int dX \mathcal{L}_{\text{sys}})$ is the generating function for free space, $\mathcal{Z}_0[J_\phi, J_\omega] = \int \mathcal{D}[\phi] \prod_{\omega} \mathcal{D}[Y_\omega] \exp\{i \int dX [\mathcal{L}_{\text{sys}} + \mathcal{L}_{\text{mat}} + J_\phi\phi + \int d\omega J_\omega Y_\omega]\}$ is the generating function for noninteracting part of the system, and J_ω and J_ϕ are source fields

that are coupled to the free fields Y_ω and ϕ , respectively. Then by integrating over ϕ and Y_m the generating function can be written as

$$\begin{aligned} \mathcal{Z}[J_\phi, J_P] &= \exp \left\{ i \int dX \int dX' \left[J_\phi G_{\phi, \phi}(X - X') J_\phi \right. \right. \\ &\quad \left. \left. + J_\phi G_{P, \phi}(X - X') J_P + J_P G_{P, P}(X - X') J_P \right] \right\}, \end{aligned} \quad (6)$$

where the Fourier transformation of the Green's function, $G_{\phi, \phi}$, is

$$G_{\phi, \phi}(q_0, \mathbf{q}) = \left[\mathbf{q}^2 - q_0^2 \left(1 + \int dq'_0 \frac{\text{sgn}[\varepsilon_1(q'_0)]\nu^2(q'_0)}{q_0'^2 - q_0'^2 + i0^+} \right) \right]^{-1}, \quad (7)$$

and for the other Green's functions can be calculated as

$$\begin{aligned} G_{\phi, P}(q_0, \mathbf{q}) &= iq_0 \int dq'_0 \frac{\text{sgn}[\varepsilon_1(q'_0)]\nu^2(q'_0)}{q_0'^2 - q_0'^2 + i0^+} G_{\phi, \phi}(q_0, \mathbf{q}), \\ G_{P, P}(q_0, \mathbf{q}) &= \left[\int dq'_0 \frac{\text{sgn}[\varepsilon_1(q'_0)]\nu^2(q'_0)}{q_0'^2 - q_0'^2 + i0^+} \right]^2 G_{\phi, \phi}(q_0, \mathbf{q}) \\ &\quad + \frac{\nu^2(q_0)}{q_0} + q_0^2, \end{aligned} \quad (8)$$

where $\vec{q} = (q_0, \mathbf{q})$, $\mathbf{q} = (q_1, q_2)$ and q_0 is the temporal Fourier component. The above Green's functions are fully in agreement with those in Refs. [30, 31]. Using the definition $\chi(q_0) = \int dq'_0 \frac{\text{sgn}[\varepsilon_1(q'_0)]\nu^2(q'_0)}{q_0'^2 - q_0'^2 + i0^+}$, it can be shown that $G_{\phi, \phi}$ is the Green's function of Eq. (2) and together with using the residues theorem, one can show that $\text{Im}\chi(q_0) = \pi \text{sgn}[\varepsilon_1(q_0)]\nu^2(q_0)/(2q_0)$. Combining $\text{Im}\chi(q_0)$ with the definitions of $G_{\phi, P}$ and $G_{P, P}$, yields $P^+ = iq_0\chi\phi^+ + P_N^+$, where $iq_0P_N^+ = j_N^+$. Here, we have assumed that the matter is homogeneous. As it has been shown in Ref. [13], among the Green's functions $G_{\phi, \phi}$, $G_{\phi, P}$ and $G_{P, P}$, only $G_{\phi, \phi}$ has contribution to the partition function and consequently to the Casimir interaction. Therefore, hereafter we drop the subscript ϕ from $G_{\phi, \phi}$. Moreover, for both amplifying and dissipative media, $G_{\phi, \phi}$ is the Green's function of Eq. (2), therefore, the Casimir interaction between ideal conductors in the presence of a dissipative or an amplifying slab (see Fig. 1) has the same mathematical form. The only difference is in the sign of $\varepsilon_1(\omega)$.

TM and TE waves can be treated as two scalar fields separately which satisfy the following differential equation $\{\nabla^2 - q_0^2 [1 + \chi(q_0, \mathbf{x})]\} \phi = 0$. For TE modes, ϕ and $\partial_z\phi$, and for TM waves, $\varepsilon(q_0)\phi$ and $\partial_z\phi$ should be continuous on the left and also on the right surfaces of the slab, and in addition, the Green's function, G , must satisfy the same BCs. Moreover, D and N BCs should be satisfied by TM and TE waves on the surfaces of both conductors, respectively.

B. Casimir interaction

To obtain the Casimir interaction, one should calculate the partition function of the system from the generating

function. To this end, Wick rotation, $x_0 \rightarrow i\tau$, on the time axis must be applied. After applying the above BCs on all fields, expressing D and N BCs in terms of path-integral over the axillary fields [11, 13, 14], and integrating over all Gaussian fields, the partition function can be cast into

$$\ln \mathcal{Z}_{\text{TM(TE)}} = -\frac{1}{2} \ln [\det \Gamma_{\text{TM(TE)}}], \quad (9)$$

where $\Gamma_{\text{TM(TE)}}$ is a second rank matrix with relevant elements of $[\Gamma_{\text{TE}}]_{\alpha\beta} = \partial_n \partial'_n G(x-y, z_\alpha(x), z_\beta(y))$, $[\Gamma_{\text{TM}}]_{\alpha\beta} = G(x-y, z_\alpha(x), z_\beta(y))$, where $\alpha, \beta = 1$ and 2 , and $z_1(x) = -H_1 - \frac{b}{2} + h_1(x)$ and $z_2(x) = H_2 + \frac{b}{2} + h_2(x)$. The Green's functions in the Fourier space can be read as

$$\begin{aligned} G_{\text{TM(TE)}}(\vec{q}, -H_1 - \frac{b}{2}, H_2 + \frac{b}{2}) &= \\ G_{\text{TM(TE)}}(\vec{q}, H_2 + \frac{b}{2}, -H_1 - \frac{b}{2}) &= \\ &= \frac{2\varepsilon_m Q_m e^{-Q_1(H_1+H_2-b)}}{(\varepsilon_m Q_1 + Q_m)^2 [-(\Delta_{1m}^{\text{TM(TE)}})^2 + e^{2Q_m b}]}, \\ G_{\text{TM(TE)}}(\vec{q}, (-1)^j(H_j + \frac{b}{2}), (-1)^j(H_j + \frac{b}{2})) &= \\ &= \frac{1}{2Q_1} - \frac{\Delta_{1m}^{\text{TM(TE)}}(-1 + e^{2Q_m b})e^{Q_1(b-2H_j)}}{2Q_1 [-(\Delta_{1m}^{\text{TM(TE)}})^2 + e^{2Q_2 b}]}, \end{aligned} \quad (10)$$

where $j = 1, 2$, $\Delta_{1m}^{\text{TM}} = \frac{Q_m - \varepsilon(iq_0)Q_1}{Q_m + \varepsilon(iq_0)Q_1}$, $\Delta_{1m}^{\text{TE}} = \frac{Q_m - Q_1}{Q_m + Q_1}$, $Q_\zeta \equiv i\sqrt{\varepsilon_\zeta(iq_0)q_0^2 + q_1^2 + q_2^2}$ with $\zeta = 1, m, 2$ corresponds to regions $z < -b/2$, $|z| < b/2$, and $z > b/2$, respectively. The dielectric function of the slab is $\varepsilon_m(iq_0) = \varepsilon(iq_0)$ while for $\zeta = 1, 2$, which corresponds to two vacuum space regions between slab and rough plates, $\varepsilon_1(iq_0) = \varepsilon_2(iq_0) = 1$. For a general case where the dielectric slab has magnetic properties in addition to the electric ones, the definition of Δ must be adjusted accordingly. The general form of Δ is presented in Appendix C.

Then, after performing the perturbative expansion up to the second order with respect to the deformation fields, $h_1(x)$ and $h_2(x)$, the partition function is written as

$$\ln \mathcal{Z}_\gamma = \ln \mathcal{Z}_{\gamma,0} + \ln \mathcal{Z}_{\gamma,2}, \quad (11)$$

where the zeroth order of the partition function in the presence of the flat bounding conductors is

$$\ln \mathcal{Z}_{\gamma,0} = -S \int \frac{d^3 \vec{q}}{(2\pi)^3} \ln K_\gamma^0(\vec{q}), \quad (12)$$

and the second order is

$$\begin{aligned} \ln \mathcal{Z}_{\gamma,2} &= \int d^3 x d^3 y \times \\ &\times \left\{ -\frac{1}{2} K_\gamma^-(x-y) [h_1(x)h_2(y) + h_2(x)h_1(y)] \right. \\ &\left. - \frac{1}{4} K_\gamma^+(x-y) \{ [h_1(x) - h_1(y)]^2 + [h_2(x) - h_2(y)]^2 \} \right\}, \end{aligned} \quad (13)$$

where the subscript, $\gamma = \text{TM}$ or TE , stands for Dirichlet or Neumann BCs, respectively. It should be mentioned that the first order term of the logarithm of the partition function vanishes because we assumed that $\int h_i(x) d^3 x = 0$, where $i = 1$ and 2 . The explicit forms of K_γ^- and K_γ^+ for the geometry depicted in Fig. 1 are presented in Appendices A and B, and the explicit forms of K_γ^0 for different geometries can be seen in Sec. III and Appendices C and D. Using Eq. (11), one can obtain the Casimir energy per unit area, S , as

$$E(H) = -\frac{\hbar c}{SL} \sum_\gamma [\ln \mathcal{Z}_\gamma(H) - \ln \mathcal{Z}_\gamma(H \rightarrow \infty)], \quad (14)$$

where L is the overall Euclidean length in the temporal direction [10]. Then, Eq. (14) is employed to study the Casimir interaction in different geometries in Secs. III and IV.

III. FLAT BOUNDARIES

In this section, we study the normal Casimir interaction between either two flat ideal conductors ($\varepsilon \rightarrow \infty$), or between a flat ideal conductor and a flat ideal permeable plate ($\mu \rightarrow \infty$), in the presence of a flat dielectric or a flat double-layer dielectric slab in between the ideal plates. Subsection III A is devoted to investigate the Casimir force between two ideal conductors in the presence of a dissipative or an amplifying slab (see Fig. 2a), or in the presence of a double-layer dielectric slab with one layer of dissipative and one layer of amplifying dielectrics (see Fig. 2b), while in subsection III B we consider the Casimir force between an ideal conductor and an ideal permeable plate in the presence of either an absorptive or an amplifying or a double-layer dielectric slab.

To this end, we model the susceptibility of the amplifying slab by Lorentz model with gain and loss which is one of the best choices to model the amplifying media [21, 24, 27]. Linear gain occurs when the medium is pumped below the lasing threshold [32]. Therefore, we consider the following model for an amplifying medium $\varepsilon_{\text{amp}}(\omega) = 1 - \frac{\omega_p^2}{\omega_0^2 - \omega^2 - i\gamma\omega}$, where $\omega_p = 0.75\omega_0$, $\gamma = 10^{-3}\omega_0$ and $\omega_0 = 10^3 \text{Hz}$ [21]. It can be shown that for amplifying media, the imaginary part of the dielectric function is negative, i.e. $\varepsilon_{\text{I,amp}}(\omega) < 0$. After applying Wick rotation, $\omega \rightarrow iq_0$, the above dielectric function is rewritten as

$$\varepsilon_{\text{amp}}(iq_0) = 1 - \frac{\omega_p^2}{\omega_0^2 + q_0^2 + \gamma q_0}. \quad (15)$$

The dielectric function of the absorptive slab is also modeled here by Lorentz-oscillator model that after applying Wick rotation can be read as

$$\varepsilon_{\text{disp}}(iq_0) = 1 + \frac{\omega_p^2}{\omega_0^2 + q_0^2 + \gamma q_0}. \quad (16)$$

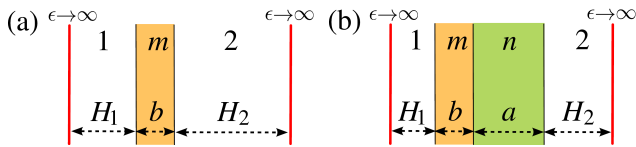


FIG. 2. (Color online) (a) Schematic picture of a dielectric slab in between two bounding ideal conductors ($\epsilon \rightarrow \infty$). The distance between the left conductor from the left side of the slab is H_1 , while the distance between the right conductor from the right side of the slab is H_2 , and the slab thickness is b . (b) Schematic picture of a double-layer dielectric slab in between two bounding ideal conductors. The left dielectric layer thickness is b , while the right dielectric layer thickness is a . The regions labeled by 1 and 2 are filled by the quantum vacuum.

A. Conductor-Conductor

To obtain the Casimir interaction between two flat conductors we set the deformation fields for both conductors to $h_1(x) = h_2(x) = 0$. Then the Casimir interaction energy per unit area for the system composed of a dielectric slab in between two flat conductors, depicted in Fig. 2a reads as

$$\frac{E_m^{\text{CC}}}{S} = \hbar c \int \frac{d^3 \vec{q}}{(2\pi)^3} \ln \left[1 + \frac{\mathcal{B}_m^{\text{TM}}}{\mathcal{D}_m^{\text{TM}}} \right] + [(\text{TM}) \rightarrow (\text{TE})], \quad (17)$$

where the index $m = \text{D}, \text{A}$ stands for a dissipative or an amplifying slab, respectively, and $\mathcal{D}_m^{\text{TM}(\text{TE})}$ and $\mathcal{B}_m^{\text{TM}(\text{TE})}$ are functions of H_1 , H_2 , b , ϵ_1 , ϵ_2 , ϵ_m (permittivities of different layers), μ_1 , μ_2 , μ_m (permeabilities of different layers), \vec{q} , and c . The explicit forms of $\mathcal{D}_m^{\text{TM}(\text{TE})}$ and $\mathcal{B}_m^{\text{TM}(\text{TE})}$ are presented in Appendix C. According to Eq. (12), the kernel at the zeroth order with respect to the deformation fields, where $h_1(x) = h_2(x) = 0$, is $K_{\text{TM}(\text{TE})}^0 = 1 + \frac{\mathcal{B}_m^{\text{TM}(\text{TE})}}{\mathcal{D}_m^{\text{TM}(\text{TE})}}$.

By using either path-integral formalism [13–15, 29] or transfer matrix method [33–35] the Casimir interaction energy per unit area for the system composed of a double-layer dielectric slab in between two flat conductors, depicted in Fig. 2b can be written as

$$\frac{E_{mn}^{\text{CC}}}{S} = \hbar c \int \frac{d^3 \vec{q}}{(2\pi)^3} \ln \left[1 + \frac{\mathcal{B}_{mn}^{\text{TM}}}{\mathcal{D}_{mn}^{\text{TM}}} \right] + [(\text{TM}) \rightarrow (\text{TE})], \quad (18)$$

where the indices $m, n = \text{D}$ and A stand for a dissipative and an amplifying slab, respectively, and $\mathcal{D}_{mn}^{\text{TM}(\text{TE})}$ and $\mathcal{B}_{mn}^{\text{TM}(\text{TE})}$ are functions of a and μ_n in addition to H_1 , H_2 , b , ϵ_1 , ϵ_2 , ϵ_m , ϵ_n , μ_1 , μ_2 , μ_m , μ_n , \vec{q} and c . The explicit forms of $\mathcal{D}_{mn}^{\text{TM}(\text{TE})}$ and $\mathcal{B}_{mn}^{\text{TM}(\text{TE})}$ are written in Appendix C.

To show the effect of the presence of the dielectric slab in between two conductors on the Casimir interaction in the system depicted in Fig. 2a, the Casimir force per unit area that the right conductor experiences at fixed H_1 and

at fixed b can be obtained as

$$\frac{F_m^{\text{CC}}}{S} = - \left. \frac{\partial E_m^{\text{CC}}}{\partial H_2} \right|_{H_1, b}. \quad (19)$$

Similar procedure is performed to calculate the Casimir force on the right conductor in the presence of the double-layer dielectrics (see Fig. 2b) as

$$\frac{F_{mn}^{\text{CC}}}{S} = - \left. \frac{\partial E_{mn}^{\text{CC}}}{\partial H_2} \right|_{H_1, a, b}. \quad (20)$$

To compare the difference between F_D^{CC} , the Casimir force in the presence of the dissipative slab, and F_A^{CC} , the Casimir force in the presence of an amplifying slab, in Fig. 3a the force per unit area has been plotted as a function of the distance between the bounding conductors, $H = H_1 + H_2 + b$, with $H_1 = H_2$, for two values of the dissipative (black solid and black dashed curves) and amplifying (red dashed-dotted and red dashed-dotted-dotted curves) slab thicknesses $b = 100$, and 125 nm . As it is clear, the force in the presence of the dissipative dielectric slab is attractive for the whole distance range between the bounding conductors, while in the presence of the amplifying slab, for small distances the force is repulsive and as the distance increases the force decreases and beyond a certain distance its sign changes and it becomes attractive. Therefore, there is an equilibrium distance, H_{equil} , where the value of the force is zero. This equilibrium distance is a function of the amplifying slab thickness, its dielectric function and the distance between the bounding conductors, H . By increasing the thickness of the amplifying slab, the location of the equilibrium point is shifted to the larger distances. The inset shows the log-log plot of $-\frac{F_m^{\text{CC}}}{S}$ as a function of H , which approximately reveals that when $H_2 > b/8$ the force scales as H^{-4} . In Fig. 3b, the Casimir force per unit area, $\frac{F_{mn}^{\text{CC}}}{S}$, in the presence of a double-layer slab between two bounding conductors depicted in Fig. 2b, has been plotted as a function of H , with $H_1 = H_2$, for two values of the dissipative and amplifying slabs thicknesses $a, b = 40$ and 50 nm . Here, $m, n = \text{D}$ and A indicate the dissipative and amplifying dielectrics, respectively. This force is attractive when both layers are dissipative (DD). When one of the layer is dissipative and the other is amplifying (DA), at small distances the force is repulsive. By increasing H , the force becomes attractive and it gets a minimum and then it grows. For DA slab the system has a mechanical equilibrium state with the equilibrium distance $H_{\text{DA, equil}}$. When both layers of the slab are amplifying (AA) the equilibrium point is shifted to the larger distances and $H_{\text{AA, equil}} > H_{\text{DA, equil}}$. The inset represents the normalized force, $F_{mn}^{\text{CC}}/|F_C|$, as a function of H . Again when approximately $H_2 > (a + b)/8$, the force scales as H^{-4} .

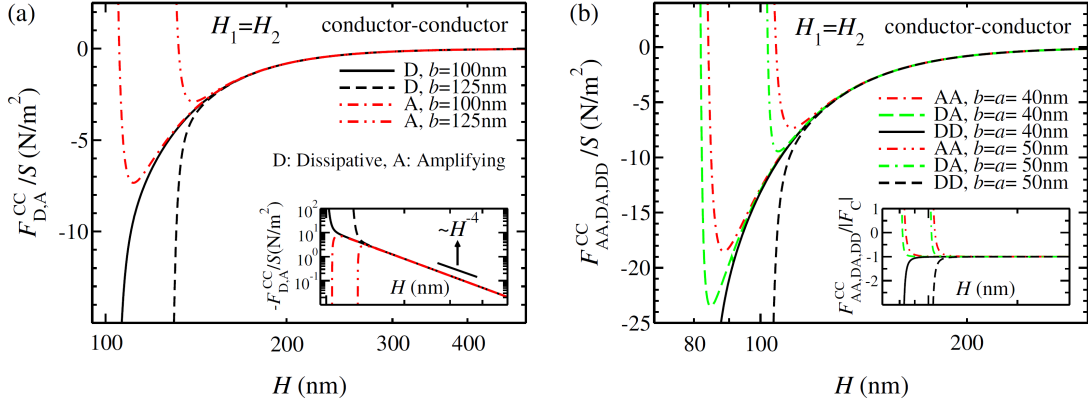


FIG. 3. (a) The force per unit area, $\frac{F_{D,A}^{CC}}{S}$, as a function of the distance between the bounding conductors, $H = H_1 + H_2 + b$, with $H_1 = H_2$, in the presence of a single dielectric slab between the bounding conductors, for two values of the dissipative (black solid and black dashed curves) and amplifying (red dashed-dotted and red dashed-dotted-dotted curves) slab thicknesses $b = 100$ and 125 nm. The inset shows the log-log plot of $-\frac{F_{D,A}^{CC}}{S}$ as a function of H . (b) The force per unit area, $\frac{F_{AA,DA,DD}^{CC}}{S}$, as a function of the distance between the bounding conductors, $H = H_1 + H_2 + a + b$, with $H_1 = H_2$, in the presence of a double layer dielectric slab between the bounding conductors, for two values of the dissipative and amplifying dielectric layers thicknesses $a = b = 40$ and 50 nm. The inset presents the normalized force $F_{mn}^{CC}/|F_C|$ as a function of H . Here, $m, n = D$ and A indicate the dissipative and amplifying dielectrics, respectively.

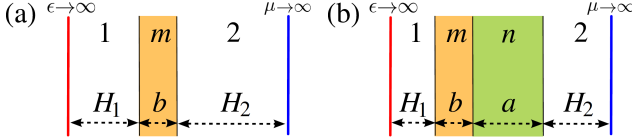


FIG. 4. (Color online) (a) Schematic picture of a dielectric slab in between two bounding plates, one is flat ideal conductor ($\epsilon \rightarrow \infty$) while the other is a flat ideal permeable plate ($\mu \rightarrow \infty$). The distance between the ideal conductor from the left side of the slab is H_1 , while the distance between the permeable plate from the right side of the slab is H_2 and the slab thickness is b . (b) Schematic picture of a double-layer dielectric slab in between an ideal conductor and an ideal permeable plate. The left dielectric layer thickness is b , while the right dielectric layer thickness is a . The regions labeled by 1 and 2 are filled by the quantum vacuum.

B. Conductor-Permeable

To observe how much the characteristics of the bounding plates can affect the Casimir interaction, we consider a system composed of a single dielectric slab, or a double-layer dielectric slab in between a flat ideal conductor in the left side and a flat ideal permeable plate in the right side of the system, depicted in Fig. 4a and b, respectively. As in 1974 Boyer showed [36], a flat conductor and a flat permeable plate immersed in the quantum vacuum and face each other at a distance H in the absence of dielectric slab, experience a repulsive force $F_B = -\frac{7}{8}F_C$ [12, 37, 38]. Here, our aim is to investigate the effect of the dissipative and amplifying slabs on the Boyer repulsive force, F_B . Using either path-integral technique [13–15, 29] or transfer matrix formalism [33–35] the Casimir

interaction energy per unit area for a system composed of a single dielectric slab in between an ideal conductor and an ideal permeable plate (see Fig. 4a) reads as

$$\frac{E_m^{CP}}{S} = \hbar c \int \frac{d^3 \vec{q}}{(2\pi)^3} \ln \left[1 + \frac{\mathcal{I}_m^{TM}}{\mathcal{J}_m^{TM}} \right] + [(TM) \rightarrow (TE)], \quad (21)$$

and for a system composed of a double-layer dielectric slab in between an ideal conductor and an ideal permeable plate (see Fig. 4b) as

$$\frac{E_{mn}^{CP}}{S} = \hbar c \int \frac{d^3 \vec{q}}{(2\pi)^3} \ln \left[1 + \frac{\mathcal{I}_{mn}^{TM}}{\mathcal{J}_{mn}^{TM}} \right] + [(TM) \rightarrow (TE)], \quad (22)$$

where again the indices $m, n = D$ and A stand for a dissipative and an amplifying slab, respectively, $\mathcal{I}_m^{TM(TE)}$ and $\mathcal{J}_m^{TM(TE)}$ are functions of $H_1, H_2, b, \epsilon_1, \epsilon_2, \epsilon_m, \mu_1, \mu_2, \mu_m, \vec{q}$ and c , and $\mathcal{I}_{mn}^{TM(TE)}$ and $\mathcal{J}_{mn}^{TM(TE)}$ are functions of the above parameters in addition to a and μ_n . The explicit forms of $\mathcal{I}_m^{TM(TE)}$, $\mathcal{J}_m^{TM(TE)}$, $\mathcal{I}_{mn}^{TM(TE)}$ and $\mathcal{J}_{mn}^{TM(TE)}$ are presented in Appendix D.

To compare the effects of a dissipative or an amplifying slab between two ideal flat plates, one conductive and the other permeable, on the Casimir interaction, the force per unit area that the permeable plate on the right side experiences can be calculated at the fixed H_1 and at fixed b as

$$\frac{F_m^{CP}}{S} = - \left. \frac{\partial E_m^{CP}}{\partial H_2} \right|_{H_1, b}. \quad (23)$$

Similar procedure can be performed to calculate the Casimir force on the right side permeable plate in the presence of the double-layer dielectric slab in between,

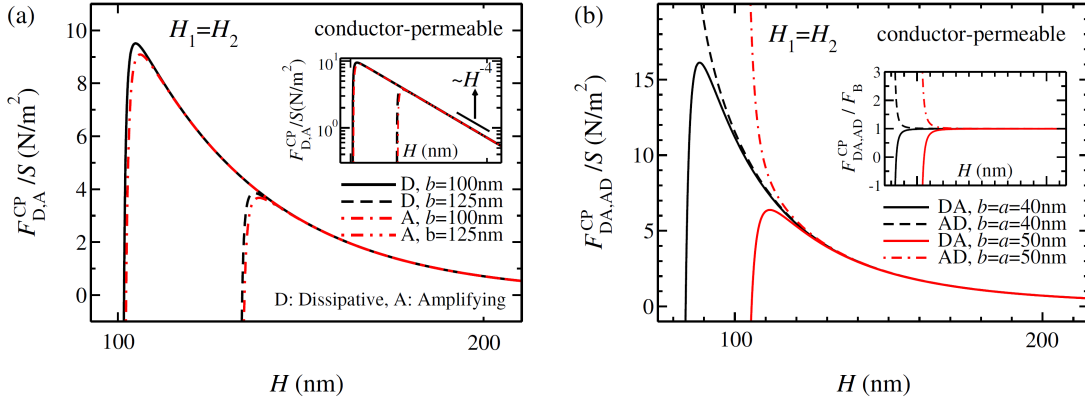


FIG. 5. (a) The force per unit area, $\frac{F_{D,A}^{CP}}{S}$, as a function of the distance between the bounding conductor and the permeable plate, $H = H_1 + H_2 + b$, with $H_1 = H_2$, in the presence of a single dielectric slab between the bounding ideal plates, for two values of the dissipative (black solid and black dashed curves) and amplifying (red dashed-dotted and red dashed-dotted-dotted curves) slab thicknesses $b = 100$ and 125 nm. The inset shows the log-log plot of $\frac{F_{D,A}^{CP}}{S}$ as a function of H . (b) The force per unit area, $\frac{F_{DA,AD}^{CP}}{S}$, as a function of the distance between the bounding ideal plates, $H = H_1 + H_2 + a + b$, with $H_1 = H_2$, in the presence of a double layer dielectric slab between the bounding ideal plates, for two values of the dissipative and amplifying slab thicknesses $a = b = 40$ and 50 nm. The inset presents the normalized force, F_{mn}^{CP}/F_B , where $F_B = -\frac{7}{8}F_C$, as a function of H . Here, $m, n = D$ and A indicate the dissipative and amplifying dielectrics, respectively.

for the fixed values of H_1, b and a , as

$$\frac{F_{mn}^{CP}}{S} = -\left. \frac{\partial E_{mn}^{CP}}{\partial H_2} \right|_{H_1, a, b}. \quad (24)$$

In Fig. 5a, the force per unit area, $\frac{F_m^{CP}}{S}$, has been plotted as a function of the distance between the bounding conductor and the permeable plate, $H = H_1 + H_2 + b$, with $H_1 = H_2$, in the presence of a single dielectric slab, for two values of the dissipative (black solid and black dashed curves) and amplifying (red dashed-dotted and red dashed-dotted-dotted curves) slabs thicknesses $b = 100$, and 125 nm. The inset shows the log-log plot of $\frac{F_m^{CP}}{S}$ as a function of H . The overall behavior of the forces due to the presence of the dissipative slab and due to the presence of the amplifying slab are similar to each other. At very small distances the bounding plates attract each other. By increasing the distance, the force increases and it gets its zero value at the distance $H_{D(A),\text{equil}}$, where $H_{D,\text{equil}} < H_{A,\text{equil}}$.

To show the effect of the asymmetry in the system due to the presence of conducting and permeable plates, on the Casimir force in the presence of the double-layer dielectric slab, the slab is located at the middle of the cavity by setting $H_1 = H_2$, and we choose $b = a$. The Casimir force is then calculated for the geometries i) conductor-vacuum-dissipative dielectric layer-amplifying dielectric layer-vacuum-permeable plate (DA), ii) conductor-vacuum-amplifying dielectric layer-dissipative dielectric layer-vacuum-permeable plate (AD). Quite interestingly, the force is different for the geometries i and ii. To present this interesting phenomenon, in Fig. 5b, the force per unit area, $\frac{F_{mn}^{CP}}{S}$, has

been plotted as a function of the distance between the bounding plates, $H = H_1 + H_2 + a + b$, for DA and AD geometries, for two values of the dissipative and amplifying slabs thicknesses $a = b = 40$ and 50 nm. The force is purely repulsive for AD geometry, while for DA, the cross over from attractive to repulsive force occurs when H increases. By increasing the thickness of the double-layer slab for DA geometry, the location of the equilibrium point is shifted to the larger distances. It should be mentioned that in both Figs. 5a and b, the equilibrium states for the position of the right ideal plate are unstable. The inset presents the normalized force, F_{mn}^{CP}/F_B , as a function of H .

IV. CORRUGATED BOUNDARIES: CONDUCTOR-CONDUCTOR

A. Normal Interaction Between a Flat and a Corrugated Conductors

To investigate the effect of corrugation on the normal Casimir interaction between two conductors in the presence of a dissipative or an amplifying slab, we set the deformation fields on the conductors $h_1(x) = 0$ and $h_2(x) = a \cos[2\pi x_1/\lambda]$ (see Fig. 1). Then the Casimir energy due to the corrugation on one of the conductors, labeled by 2, is obtained as

$$E_{CF} = \frac{\hbar c}{AL} \sum_{\gamma} [\ln \mathcal{Z}_{\gamma,2}(H) - \ln \mathcal{Z}_{\gamma,2}(H \rightarrow \infty)]|_{h_1(x)=0}, \quad (25)$$

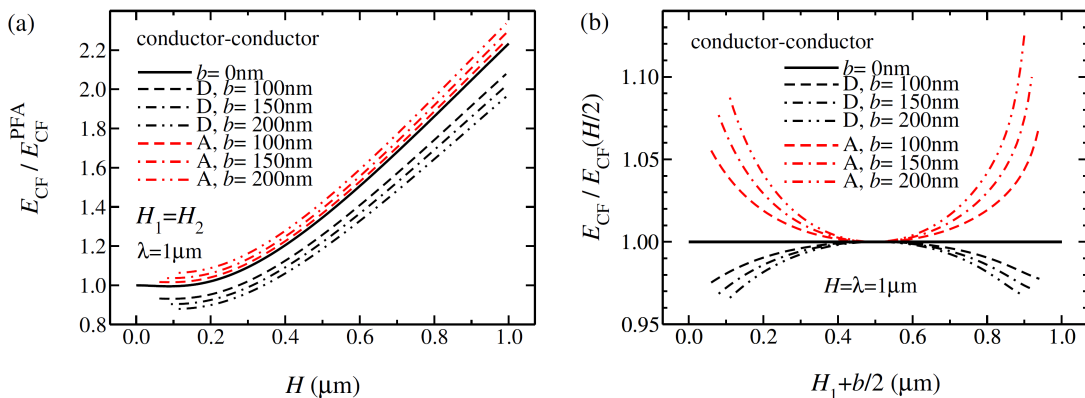


FIG. 6. (a) The normalized Casimir energy, E_{CF}/E_{CF}^{PFA} , as a function of $H = H_1 + H_2 + b$ with $H_1 = H_2$ and $\lambda = 1 \mu\text{m}$ in the presence of a dissipative (D, black curves) or an amplifying (A, red curves) dielectric slab for various values of the slab thicknesses $b = 0, 100, 150$ and 200 nm. The black solid curve shows the normalized energy in the absence of dielectric slab. (b) The normalized Casimir energy, $\frac{E_{CF}}{E_{CF}(H/2)}$, as a function of $H_1 + b/2$ which is the distance between the left conductor and the middle of the absorptive (black curves) and amplifying slabs (red curves), for fixed values of $\lambda = H = 1 \mu\text{m}$ and different values of b the same as those of panel (a). Here, $E_{CF}(H/2)$ is the value of E_{CF} when the center of the slab is located at the distance $H/2$ from each conductors. i.e. $H_1 = H_2$.

where index CF stands for corrugated-flat, and sum is over $\gamma = \text{TM}$ and TE . This energy can then be cast into

$$E_{CF} = -\frac{\pi^2 a^2 \hbar c}{240 H^5} \left[K_{\text{TM}}^{+\text{reg}}\left(\frac{H}{\lambda}\right) + K_{\text{TE}}^{+\text{reg}}\left(\frac{H}{\lambda}\right) \right], \quad (26)$$

where according to Eq. (25), the regular part of the TM and TE kernels is defined as $K_{\text{TM}(\text{TE})}^{+\text{reg}} = K_{\text{TM}(\text{TE})}^+ - \lim_{H_1 \rightarrow \infty} K_{\text{TM}(\text{TE})}^+$. In Eq. (26), $K_{\text{TM}(\text{TE})}^+(q)$ is the Fourier transformation of $K_{\text{TM}(\text{TE})}^+(x)$ at $\vec{q} = (0, \frac{2\pi}{\lambda}, 0)$. The explicit forms of $K_{\text{TM}}^+(\frac{H}{\lambda})$ and $K_{\text{TE}}^+(\frac{H}{\lambda})$ are presented in Appendices A and B. In Fig. 6a the normalized contribution of the corrugation to the Casimir energy, $\frac{E_{CF}^{PFA}}{E_{CF}}$, has been plotted as a function of $H = H_1 + H_2 + b$ with $H_1 = H_2$ and $\lambda = 1 \mu\text{m}$ in the presence of a dissipative (D, black curves) or an amplifying (A, red curves) dielectric slab with thicknesses $b = 0, 100, 150$ and 200 nm. The black solid curve shows the normalized energy in the absence of dielectric slab. Quite interestingly, the presence of an amplifying slab enhances the Casimir interaction due to the roughness while the interaction is weakened by the presence of the absorptive slab. This effect is more pronounced by increasing the slab thickness. The dielectric functions of the amplifying and dissipative slabs are the same as of Eqs. (15) and (16), respectively.

The superscript PFA in E_{CF}^{PFA} stands for proximity force approximation. PFA is used when a , which is the corrugation amplitude, is much smaller than the other length scales in the system such as H and λ . In the proximity force approximation, the surface elements of a curved surface around each point are simply replaced by surface elements parallel to the plane of (x_1, x_2) at the same point [39, 40]. The Casimir energy in a system composed of a corrugated and a flat conductors in PFA

$$\text{is } E_{CF}^{PFA} = -\frac{a^2}{4} \frac{\partial F_C}{\partial H}.$$

To study the effect of the location of the dielectric slab on the Casimir interaction between the bounding plates, in Fig. 6b, the normalized Casimir energy, $\frac{E_{CF}}{E_{CF}(H/2)}$, has been shown as a function of $H_1 + b/2$ which is the distance between the left conductor and the middle of the dissipative slab (black curves) or the middle of the amplifying slab (red curves), for fixed values of $\lambda = H = 1 \mu\text{m}$ and different values of b which are the same as those of panel (a). Here, $E_{CF}(H/2)$ is the value of E_{CF} when the center of the slab is located at the distance $H/2$ from each conductors. As it can be seen, when the amplifying slab is closer to the rough conductor in the right side, this effect is more pronounced.

B. Lateral Force Between Two Corrugated Conductors

Two corrugated conductors, immersed in the quantum vacuum, can experience the lateral Casimir force due to the translational symmetry breaking [10, 11, 16] in addition to the normal Casimir force. In this section, we compare the effect of the presence of the absorptive or amplifying dielectric slabs on the lateral Casimir force between the bounding corrugated conductors depicted in Fig. 1. The lateral Casimir force is calculated by $F_l = -\frac{\partial E}{\partial l}$, where E is the Casimir energy in Eq. (14). By setting the corrugation fields on the rough conductors depicted in Fig. 1 as $h_1(x) = a \cos[2\pi x_1/\lambda]$ and $h_2(x) = a \cos[2\pi(x_1 + l)/\lambda]$, the lateral Casimir force is then obtained as

$$F_l = \frac{2\pi \hbar c a^2}{\lambda H^5} \sin\left(\frac{2\pi l}{\lambda}\right) \left[K_{\text{TM}}^-\left(\frac{H}{\lambda}\right) + K_{\text{TE}}^-\left(\frac{H}{\lambda}\right) \right], \quad (27)$$

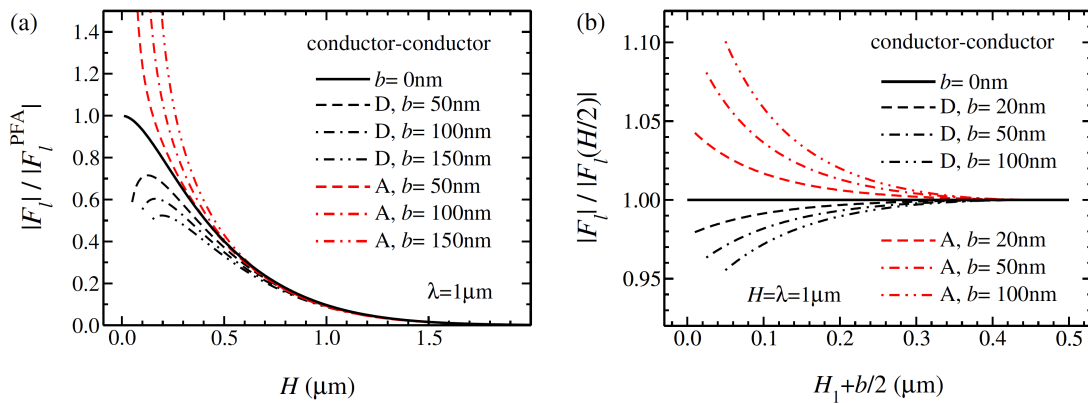


FIG. 7. (a) The normalized amplitude of the lateral Casimir force, $|F_l|/|F_l^{\text{PFA}}|$, between rough metallic plates (depicted in Fig. 1) as a function of the mean distance between corrugated conductors, $H = H_1 + H_2 + b$, for fixed corrugation wavelength $\lambda = 1 \mu\text{m}$, and various values of dissipative slab thicknesses $b = 0, 50, 100$ and 150 nm (black curves, from top to bottom) and amplifying slab thicknesses (red curves, from bottom to top) the same as of the dissipative one. Here, the center of the slab is fixed at the middle distance between bounding ideal conductors. (b) The normalized amplitude of the lateral Casimir force, $|F_l|/|F_l(H/2)|$, as a function of $H_1 + b/2$ which is the distance between the left conductor and the middle of the dissipative (black curves) or amplifying slab (red curves), for fixed values of $\lambda = H = 1 \mu\text{m}$ and different values of the dielectric slab thicknesses $b = 0, 20, 50$ and 100 nm. Here, $|F_l(H/2)|$ is the amplitude of the lateral force when the center of the slab is located at the distance $H/2$ from each conductors.

where $K_{\text{TM}}^-(q)$ and $K_{\text{TE}}^-(q)$ are the Fourier transformations of $K_{\text{TM}}^-(x)$ and $K_{\text{TE}}^-(x)$ at $\vec{q} = (0, \frac{2\pi}{\lambda}, 0)$, respectively, and their explicit forms can be seen in Appendices A and B.

In Fig. 7(a), we have plotted the normalized amplitude of the lateral Casimir force, $|F_l|/|F_l^{\text{PFA}}|$, between two rough metallic plates depicted in Fig. 1 as a function of H (the mean separation distance between corrugated conductors) for fixed corrugation wavelength, $\lambda = 1 \mu\text{m}$ and various values of the absorptive (black curves) amplifying (red curves) slabs thicknesses $b = 0, 50, 100$ and 150 nm. Here, the center of the slab is fixed at the middle distance between plates. $|F_l^{\text{PFA}}|$ is the magnitude of the lateral Casimir force for the same geometry in PFA [39, 40], which is $|F_l^{\text{PFA}}| = \frac{\pi a^2}{\lambda} \frac{\partial F_C}{\partial H}$. Comparing the value of the normalized lateral Casimir force in the presence of the dissipative and amplifying slabs yields that at small distances, the lateral Casimir force in the presence of an amplifying slab is stronger than that of absorptive dielectric slab with the same thickness, whereas by increasing the distance, in both cases, the values of the normalized force approach to the values of the force in the absence of the dielectric slab. Moreover, by increasing the thickness of an amplifying slab, the lateral Casimir force increases whereas for the absorptive one decreases.

We have also considered the effect of the location of the center of the dissipative or amplifying slabs, $H_1 + b/2$, on the lateral Casimir force. To this end, in Fig. 7b, the normalized amplitude of the lateral Casimir force, $|F_l|/|F_l(H/2)|$, has been shown as a function of $H_1 + b/2$ which is the mean distance between the left conductor and the middle of the dissipative (black curves) or amplifying (red curves) slab, for fixed values of $\lambda = H = 1 \mu\text{m}$

and different values of $b = 0, 20, 50$ and 100 nm. $|F_l(H/2)|$ is the amplitude of the lateral force when the center of the slab is fixed at the middle of the cavity. The dielectric functions of the amplifying and absorptive slabs are chosen the same as in Eqs. (15) and (16), respectively. The sinusoidal behavior of the force does not alter by changing H_1 , while its amplitude alters. Moreover, if the amplifying slab comes closer to each conductor, the amplitude of the lateral Casimir force increases. In contrast to the amplifying slab, the amplitude of the lateral Casimir force decreases when the dissipative dielectrics comes closer to one of the bounding conductors. By increasing the thickness of the slab, this effect is more pronounced.

V. CONCLUSION

Using either path-integral formalism or transfer matrix method, we investigated the normal Casimir interaction between flat ideal plates in the presence of a dissipative or an amplifying slab, or a double-layer dielectric slab. The normal force between flat ideal conductors is non-monotonic due to the presence of the amplifying slab and the system has a stable equilibrium state, while the force is attractive and is weakened by intervening the absorptive dielectric slab in the cavity. By replacing the right flat conductor by an ideal permeable plate, the overall behaviors of the Casimir force in the presence of the absorptive slab and in the presence of the amplifying slab are the same, and for both cases, the force is non-monotonic and the system has an unstable equilibrium state. Quite interestingly, the Casimir force is non-monotonic in the presence of a double-layer di-

electric slab in the DA geometry while it is purely repulsive for the AD geometry. Then employing the path-integral technique, we calculated the correction to the normal Casimir interaction due to the corrugation on one of the bounding conductors, and also the lateral Casimir force has been obtained due to the roughness on both bounding conductors in the presence of the absorptive or amplifying slab. While the presence of the amplifying slab enhances both normal and lateral Casimir interactions between the bounding conductors due to the roughness, the presence of the absorptive slab weakens both normal and lateral interactions compared to those of a cavity contains only vacuum between the bounding conductors. We also showed that both normal and lateral Casimir interactions depend on the distance of the slab from the bounding conductors. By approaching the amplifying slab to one of the conductors, both normal and lateral Casimir interactions enhance compared to the Casimir interactions in a cavity which contains only vacuum between the bounding conductors. If instead, the dissipative dielectric slab is brought closer to one of the bounding conductors both normal and lateral Casimir interactions are weakened. The reason for the difference in

the behavior of the Casimir interactions can be understood if one looks at the characteristics of the vacuum fluctuations of the EM field near the slab. The dissipative medium decreases the vacuum fluctuations of the EM field whereas the amplifying medium increases these fluctuations [24, 41]. The method that we employed in this paper can be used to study the dynamic Casimir effect [11, 43] and the Casimir interaction at finite temperature [35, 44] in the presence of absorptive or amplifying slabs.

ACKNOWLEDGMENTS

J.S. acknowledges support from the Academy of Finland through its Centers of Excellence Program (2012-2017) under Project No. 915804.

Appendix A: Fourier transformation of $K_{\text{TM}}^{+(-)}(x)$

The Fourier transformations of the kernels for TM waves at $(0, \frac{2\pi}{\lambda}, 0)$ are

$$\begin{aligned}
K_{\text{TM}}^+(0, \frac{2\pi}{\lambda}, 0) &= \int \frac{d^3\vec{q}}{(2\pi)^3} \left[+F_1(\vec{q}, H_1, H_1)Q_1^2G_{\text{TM}}(\vec{q} + \frac{2\pi}{\lambda}\hat{i}, H_2 + \frac{b}{2}, H_2 + \frac{b}{2}) + F_1(\vec{q}, H_1, H_1)F_5(\vec{q} + \frac{2\pi}{\lambda}\hat{i}, H_2, H_2) \right. \\
&\quad \left. + F_3(\vec{q}, H_1, H_1)F_3(\vec{q} + \frac{2\pi}{\lambda}\hat{i}, H_2, H_2) \right], \\
K_{\text{TM}}^-(0, \frac{2\pi}{\lambda}, 0) &= \int \frac{d^3\vec{q}}{(2\pi)^3} \left[+F_2(\vec{q}, H_1, H_1)Q_1^2G_{\text{TM}}(\vec{q} + \frac{2\pi}{\lambda}\hat{i}, H_2 + \frac{b}{2}, H_2 + \frac{b}{2}) + F_4(\vec{q}, H_1, H_1)F_6(\vec{q} + \frac{2\pi}{\lambda}\hat{i}, H_2, H_2) \right. \\
&\quad \left. + F_2(\vec{q}, H_1, H_1)F_2(\vec{q} + \frac{2\pi}{\lambda}\hat{i}, H_2, H_2) \right], \tag{A1}
\end{aligned}$$

where

$$\begin{aligned}
F_1(\vec{q}, H_i, H_i) &= \frac{G_{\text{TM}}(\vec{q}, (-1)^i(H_i + \frac{b}{2}), (-1)^i(H_i + \frac{b}{2}))}{N(\vec{q}, H_1, H_2)}, \\
F_2(\vec{q}, H_i, H_i) &= \frac{G_{\text{TM}}(\vec{q}, (-1)^i(H_i + \frac{b}{2}), (-1)^i(H_i + \frac{b}{2}))}{N(\vec{q}, H_1, H_2)}Q_1G_{\text{TM}}(\vec{q}, -H_1 - \frac{b}{2}, H_2 + \frac{b}{2}), \\
F_3(\vec{q}, H_1, H_2) &= \frac{G_{\text{TM}}(\vec{q}, -H_1 - \frac{b}{2}, H_2 + \frac{b}{2})}{N(\vec{q}, H_1, H_2)}Q_1G_{\text{TM}}(\vec{q}, -H_1 - \frac{b}{2}, H_2 + \frac{b}{2}), \\
F_4(\vec{q}, H_1, H_2) &= \frac{G_{\text{TM}}(\vec{q}, -H_1 - \frac{b}{2}, H_2 + \frac{b}{2})}{N(\vec{q}, H_1, H_2)}, \\
F_5(\vec{q}, H_i, H_i) &= \frac{G_{\text{TM}}(\vec{q}, (-1)^i(H_i + \frac{b}{2}), (-1)^i(H_i + \frac{b}{2}))}{N(\vec{q}, H_1, H_2)}Q_1^2G_{\text{TM}}(\vec{q}, -H_1 - \frac{b}{2}, H_2 + \frac{b}{2}), \\
F_6(\vec{q}, H_1, H_2) &= \frac{G_{\text{TM}}(\vec{q}, -H_1 - \frac{b}{2}, H_2 + \frac{b}{2})}{N(\vec{q}, H_1, H_2)}Q_1^2G_{\text{TM}}(\vec{q}, -H_1 - \frac{b}{2}, H_2 + \frac{b}{2}), \tag{A2}
\end{aligned}$$

and

$$N(\vec{q}, H_1, H_2) = G_{\text{TM}}(\vec{q}, -H_1 - \frac{b}{2}, -H_1 - \frac{b}{2})G_{\text{TM}}(\vec{q}, H_2 + \frac{b}{2}, H_2 + \frac{b}{2}) - G_{\text{TM}}^2(\vec{q}, -H_1 - \frac{b}{2}, H_2 + \frac{b}{2}). \tag{A3}$$

Appendix B: Fourier transformation of $K_{\text{TE}}^{-(+)}(x)$

The Fourier transformations of the kernels for TE waves at $(0, \frac{2\pi}{\lambda}, 0)$ are

$$\begin{aligned}
K_{\text{TE}}^+(0, \frac{2\pi}{\lambda}, 0) &= \int \frac{d^3\vec{q}}{(2\pi)^3} \left\{ \mathcal{F}_1(\vec{q}, H_1, H_1) Q_1^2 g(\vec{q} + \frac{2\pi}{\lambda}\hat{i}, H_2, H_2) + \mathcal{F}_1(\vec{q}, H_1, H_1) \mathcal{F}_5(\vec{q} + \frac{2\pi}{\lambda}\hat{i}, H_2, H_2) \right. \\
&+ \mathcal{F}_3(\vec{q}, H_1, H_2) \mathcal{F}_3(\vec{q} + \frac{2\pi}{\lambda}\hat{i}, H_1, H_2) + (\frac{2\pi}{\lambda})^2 \left[\mathcal{F}_1(\vec{q}, H_1, H_1) (q_1 + \frac{2\pi}{\lambda})^2 G_{\text{TE}}(\vec{q} + \frac{2\pi}{\lambda}\hat{i}, H_2 + \frac{b}{2}, H_2 + \frac{b}{2}) \right. \\
&+ \mathcal{F}_1(\vec{q}, H_1, H_1) (q_1 + \frac{2\pi}{\lambda})^2 \mathcal{F}_7(\vec{q} + \frac{2\pi}{\lambda}\hat{i}, H_2, H_2) + q_1 (q_1 + \frac{2\pi}{\lambda}) \mathcal{F}_9(\vec{q}, H_1, H_2) \mathcal{F}_9(\vec{q} + \frac{2\pi}{\lambda}\hat{i}, H_1, H_2) \left. \right] \\
&+ \frac{2\pi}{\lambda} \left[\mathcal{F}_1(\vec{q}, H_1, H_1) (q_1 + \frac{2\pi}{\lambda}) g(\vec{q} + \frac{2\pi}{\lambda}\hat{i}, H_2, H_2) + \mathcal{F}_1(\vec{q}, H_1, H_1) (q_1 + \frac{2\pi}{\lambda}) \mathcal{F}_{11}(\vec{q} + \frac{2\pi}{\lambda}\hat{i}, H_2, H_2) \right. \\
&+ \left. \left. \mathcal{F}_2(\vec{q}, H_1, H_1) (q_1 + \frac{2\pi}{\lambda}) \mathcal{F}_{10}(\vec{q} + \frac{2\pi}{\lambda}\hat{i}, H_2, H_2) \right] \right\}, \\
K_{\text{TE}}^-(0, \frac{2\pi}{\lambda}, 0) &= \int \frac{d^3\vec{q}}{(2\pi)^3} \left\{ \mathcal{F}_4(\vec{q}, H_1, H_2) Q_1^2 g(\vec{q} + \frac{2\pi}{\lambda}\hat{i}, H_2, H_2) + \mathcal{F}_4(\vec{q}, H_1, H_2) \mathcal{F}_6(\vec{q} + \frac{2\pi}{\lambda}\hat{i}, H_1, H_2) \right. \\
&+ \mathcal{F}_2(\vec{q}, H_1, H_1) \mathcal{F}_2(\vec{q} + \frac{2\pi}{\lambda}\hat{i}, H_2, H_2) + (\frac{2\pi}{\lambda})^2 \left[\mathcal{F}_4(\vec{q}, H_1, H_2) (q_1 + \frac{2\pi}{\lambda})^2 G_{\text{TE}}(\vec{q} + \frac{2\pi}{\lambda}\hat{i}, H_2 + \frac{b}{2}, H_2 + \frac{b}{2}) \right. \\
&+ \mathcal{F}_4(\vec{q}, H_1, H_2) (q_1 + \frac{2\pi}{\lambda})^2 \mathcal{F}_8(\vec{q} + \frac{2\pi}{\lambda}\hat{i}, H_1, H_2) + q_1 (q_1 + \frac{2\pi}{\lambda}) \mathcal{F}_{10}(\vec{q}, H_1, H_1) \mathcal{F}_{10}(\vec{q} + \frac{2\pi}{\lambda}\hat{i}, H_1, H_2) \left. \right] \\
&+ 2\frac{2\pi}{\lambda} \left[\mathcal{F}_4(\vec{q}, H_1, H_2) (q_1 + \frac{2\pi}{\lambda}) g(\vec{q} + \frac{2\pi}{\lambda}\hat{i}, H_1, H_2) + \mathcal{F}_4(\vec{q}, H_1, H_2) (q_1 + \frac{2\pi}{\lambda}) \mathcal{F}_{12}(\vec{q} + \frac{2\pi}{\lambda}\hat{i}, H_1, H_2) \right. \\
&+ \left. \left. \mathcal{F}_2(\vec{q}, H_1, H_1) (q_1 + \frac{2\pi}{\lambda}) \mathcal{F}_{10}(\vec{q} + \frac{2\pi}{\lambda}\hat{i}, H_2, H_2) \right] \right\}, \tag{B1}
\end{aligned}$$

where

$$\begin{aligned}
\mathcal{F}_1(\vec{q}, H_i, H_i) &= \frac{g(\vec{q}, H_i, H_i)}{\mathcal{N}(\vec{q}, H_1, H_2)}, \\
\mathcal{F}_2(\vec{q}, H_i, H_i) &= \frac{g(\vec{q}, H_i, H_i)}{\mathcal{N}(\vec{q}, H_1, H_2)} Q_1 g(\vec{q}, H_1, H_2), \\
\mathcal{F}_3(\vec{q}, H_1, H_2) &= \frac{g(\vec{q}, H_1, H_2)}{\mathcal{N}(\vec{q}, H_1, H_2)} Q_1 g(\vec{q}, H_1, H_2), \\
\mathcal{F}_4(\vec{q}, H_1, H_2) &= \frac{g(\vec{q}, H_1, H_2)}{\mathcal{N}(\vec{q}, H_1, H_2)}, \\
\mathcal{F}_5(\vec{q}, H_i, H_i) &= \frac{g(\vec{q}, H_i, H_i)}{\mathcal{N}(\vec{q}, H_1, H_2)} Q_1^2 g(\vec{q}, H_1, H_2), \\
\mathcal{F}_6(\vec{q}, H_1, H_2) &= \frac{g(\vec{q}, H_1, H_2)}{\mathcal{N}(\vec{q}, H_1, H_2)} Q_1^2 g(\vec{q}, H_1, H_2), \\
\mathcal{F}_7(\vec{q}, H_i, H_i) &= \frac{g(\vec{q}, H_i, H_i)}{\mathcal{N}(\vec{q}, H_1, H_2)} Q_1^2 \\
&\quad \times G_{\text{TE}}(\vec{q}, -H_1 - \frac{b}{2}, H_2 + \frac{b}{2}), \\
\mathcal{F}_8(\vec{q}, H_1, H_2) &= \frac{g(\vec{q}, H_1, H_2)}{\mathcal{N}(\vec{q}, H_1, H_2)} Q_1^2 \\
&\quad \times G_{\text{TE}}(\vec{q}, -H_1 - \frac{b}{2}, H_2 + \frac{b}{2}), \tag{B2}
\end{aligned}$$

$$\begin{aligned}
\mathcal{F}_9(\vec{q}, H_1, H_2) &= \frac{g(\vec{q}, H_1, H_2)}{\mathcal{N}(\vec{q}, H_1, H_2)} Q_1 \\
&\quad \times G_{\text{TE}}(\vec{q}, -H_1 - \frac{b}{2}, H_2 + \frac{b}{2}), \\
\mathcal{F}_{10}(\vec{q}, H_i, H_i) &= \frac{g(\vec{q}, H_i, H_i)}{\mathcal{N}(\vec{q}, H_1, H_2)} Q_1 \\
&\quad \times G_{\text{TE}}(\vec{q}, -H_1 - \frac{b}{2}, H_2 + \frac{b}{2}), \\
\mathcal{F}_{11}(\vec{q}, H_i, H_i) &= \frac{g(\vec{q}, H_i, H_i)}{\mathcal{N}(\vec{q}, H_1, H_2)} Q_1 \\
&\quad \times G_{\text{TE}}(\vec{q}, -H_1 - \frac{b}{2}, H_2 + \frac{b}{2}) Q_1 g(\vec{q}, H_1, H_2), \\
\mathcal{F}_{12}(\vec{q}, H_1, H_2) &= \frac{g(\vec{q}, H_1, H_2)}{\mathcal{N}(\vec{q}, H_1, H_2)} Q_1 \\
&\quad \times G_{\text{TE}}(\vec{q}, -H_1 - \frac{b}{2}, H_2 + \frac{b}{2}) Q_1 g(\vec{q}, H_1, H_2), \tag{B3}
\end{aligned}$$

and

$$\begin{aligned}
g(\vec{q}, H_i, H_j) &= Q_1^2 G_{\text{TE}}(\vec{q}, (-1)^i (H_i + \frac{b}{2}), (-1)^j (H_j + \frac{b}{2})), \tag{B4} \\
\mathcal{N}(\vec{q}, H_1, H_2) &= g(\vec{q}, H_1, H_1) g(\vec{q}, H_2, H_2) - g^2(\vec{q}, H_1, H_2). \tag{B5}
\end{aligned}$$

Appendix C: Conductor-Conductor

The definitions of $\mathcal{B}_m^{\text{TM}}$, $\mathcal{B}_m^{\text{TE}}$, $\mathcal{D}_m^{\text{TM}}$ and $\mathcal{D}_m^{\text{TE}}$ are

$$\begin{aligned}
\mathcal{B}_m^{\text{TM}} &= -\Delta_{m1}^{\text{TM}} e^{-2Q_1 H_1} + \Delta_{2m}^{\text{TM}} e^{-2Q_2 H_2} - \Delta_{m1}^{\text{TM}} \Delta_{2m}^{\text{TM}} e^{-2(Q_1 H_1 + Q_2 H_2)} - \Delta_{2m}^{\text{TM}} e^{-2(Q_1 H_1 + Q_m b)} + \Delta_{m1}^{\text{TM}} e^{-2(Q_2 H_2 + Q_m b)} \\
&\quad - e^{-2(Q_1 H_1 + Q_2 H_2 + Q_m b)}, \\
\mathcal{D}_m^{\text{TM(TE)}} &= 1 + \Delta_{m1}^{\text{TM(TE)}} \Delta_{2m}^{\text{TM(TE)}} e^{-2Q_m b}, \\
\mathcal{B}_m^{\text{TE}} &= +\Delta_{m1}^{\text{TE}} e^{-2Q_1 H_1} - \Delta_{2m}^{\text{TE}} e^{-2Q_2 H_2} - \Delta_{m1}^{\text{TE}} \Delta_{2m}^{\text{TE}} e^{-2(Q_1 H_1 + Q_2 H_2)} + \Delta_{2m}^{\text{TE}} e^{-2(Q_1 H_1 + Q_m b)} - \Delta_{m1}^{\text{TE}} e^{-2(Q_2 H_2 + Q_m b)} \\
&\quad - e^{-2(Q_1 H_1 + Q_2 H_2 + Q_m b)},
\end{aligned} \tag{C1}$$

where

$$\Delta_{ij}^{\text{TM}} = \frac{\varepsilon_i(\nu q_0) Q_j(\nu q_0) - \varepsilon_j(\nu q_0) Q_i(\nu q_0)}{\varepsilon_i(\nu q_0) Q_j(\nu q_0) + \varepsilon_j(\nu q_0) Q_i(\nu q_0)}, \quad \Delta_{ij}^{\text{TE}} = \frac{\mu_i(\nu q_0) Q_j(\nu q_0) - \mu_j(\nu q_0) Q_i(\nu q_0)}{\mu_i(\nu q_0) Q_j(\nu q_0) + \mu_j(\nu q_0) Q_i(\nu q_0)}, \tag{C2}$$

with the layer labeled by j is located at the left-hand side of the layer labeled by i . $Q_i^2 = \mathbf{q}^2 + \frac{\varepsilon_i(\nu q_0) \mu_i(\nu q_0) q_0^2}{c^2}$, $\mathbf{q}^2 = q_1^2 + q_2^2$ and c is the speed of light in the vacuum. Functions $\mathcal{B}_{mn}^{\text{TM}}$, $\mathcal{B}_{mn}^{\text{TE}}$, $\mathcal{D}_{mn}^{\text{TM}}$ and $\mathcal{D}_{mn}^{\text{TE}}$ are

$$\begin{aligned}
\mathcal{B}_{mn}^{\text{TM}} &= +\Delta_{2n}^{\text{TM}} e^{-2Q_2 H_2} + \Delta_{nm}^{\text{TM}} e^{-2(Q_n a + Q_2 H_2)} - \Delta_{m1}^{\text{TM}} e^{-2Q_1 H_1} - \Delta_{2n}^{\text{TM}} \Delta_{m1}^{\text{TM}} e^{-2(Q_1 H_1 + Q_2 H_2)} \\
&\quad - \Delta_{2n}^{\text{TM}} \Delta_{nm}^{\text{TM}} \Delta_{m1}^{\text{TM}} e^{-2(Q_n a + Q_1 H_1)} - \Delta_{nm}^{\text{TM}} \Delta_{m1}^{\text{TM}} e^{-2(Q_1 H_1 + Q_2 H_2 + Q_n a)} - \Delta_{nm}^{\text{TM}} e^{-2(Q_m b + Q_1 H_1)} \\
&\quad + \Delta_{2n}^{\text{TM}} \Delta_{nm}^{\text{TM}} \Delta_{m1}^{\text{TM}} e^{-2(Q_m b + Q_2 H_2)} - \Delta_{2n}^{\text{TM}} \Delta_{nm}^{\text{TM}} e^{-2(Q_1 H_1 + Q_2 H_2 + Q_m b)} - \Delta_{2n}^{\text{TM}} e^{-2(Q_n a + Q_m b + Q_1 H_1)} \\
&\quad + \Delta_{m1}^{\text{TM}} e^{-2(Q_n a + Q_m b + Q_2 H_2)} - e^{-2(Q_1 H_1 + Q_2 H_2 + Q_n a + Q_m b)}, \\
\mathcal{D}_{mn}^{\text{TM(TE)}} &= 1 + \Delta_{2n}^{\text{TM(TE)}} \Delta_{nm}^{\text{TM(TE)}} e^{-2Q_n a} + \Delta_{m1}^{\text{TM(TE)}} \Delta_{nm}^{\text{TM(TE)}} e^{-2Q_m b} + \Delta_{2n}^{\text{TM(TE)}} \Delta_{m1}^{\text{TM(TE)}} e^{-2(Q_n a + Q_m b)}, \\
\mathcal{B}_{mn}^{\text{TE}} &= -\Delta_{2n}^{\text{TE}} e^{-2Q_2 H_2} - \Delta_{nm}^{\text{TE}} e^{-2(Q_n a + Q_2 H_2)} + \Delta_{m1}^{\text{TE}} e^{-2Q_1 H_1} - \Delta_{2n}^{\text{TE}} \Delta_{m1}^{\text{TE}} e^{-2(Q_1 H_1 + Q_2 H_2)} \\
&\quad + \Delta_{2n}^{\text{TE}} \Delta_{nm}^{\text{TE}} \Delta_{m1}^{\text{TE}} e^{-2(Q_n a + Q_1 H_1)} - \Delta_{nm}^{\text{TE}} \Delta_{m1}^{\text{TE}} e^{-2(Q_1 H_1 + Q_2 H_2 + Q_n a)} + \Delta_{nm}^{\text{TE}} e^{-2(Q_m b + Q_1 H_1)} \\
&\quad - \Delta_{2n}^{\text{TE}} \Delta_{nm}^{\text{TE}} \Delta_{m1}^{\text{TE}} e^{-2(Q_m b + Q_2 H_2)} - \Delta_{2n}^{\text{TE}} \Delta_{nm}^{\text{TE}} e^{-2(Q_1 H_1 + Q_2 H_2 + Q_m b)} + \Delta_{2n}^{\text{TE}} e^{-2(Q_n a + Q_m b + Q_1 H_1)} \\
&\quad - \Delta_{m1}^{\text{TE}} e^{-2(Q_n a + Q_m b + Q_2 H_2)} - e^{-2(Q_1 H_1 + Q_2 H_2 + Q_n a + Q_m b)}.
\end{aligned} \tag{C3}$$

Appendix D: Conductor-Permeable

Functions $\mathcal{I}_m^{\text{TM}}$, $\mathcal{I}_m^{\text{TE}}$, $\mathcal{J}_m^{\text{TM}}$, $\mathcal{J}_m^{\text{TE}}$, $\mathcal{I}_{mn}^{\text{TM}}$, $\mathcal{I}_{mn}^{\text{TE}}$, $\mathcal{J}_{mn}^{\text{TM}}$ and $\mathcal{J}_{mn}^{\text{TE}}$ are

$$\begin{aligned}
\mathcal{I}_m^{\text{TM}} &= -\Delta_{m1}^{\text{TM}} e^{-2Q_1 H_1} - \Delta_{2m}^{\text{TM}} e^{-2Q_2 H_2} + \Delta_{m1}^{\text{TM}} \Delta_{2m}^{\text{TM}} e^{-2(Q_1 H_1 + Q_2 H_2)} - \Delta_{2m}^{\text{TM}} e^{-2(Q_1 H_1 + Q_m b)} - \Delta_{m1}^{\text{TM}} e^{-2(Q_2 H_2 + Q_m b)} \\
&\quad + e^{-2(Q_1 H_1 + Q_2 H_2 + Q_m b)}, \\
\mathcal{J}_m^{\text{TM(TE)}} &= 1 + \Delta_{m1}^{\text{TM(TE)}} \Delta_{2m}^{\text{TM(TE)}} e^{-2Q_m b}, \\
\mathcal{I}_m^{\text{TE}} &= +\Delta_{m1}^{\text{TE}} e^{-2Q_1 H_1} + \Delta_{2m}^{\text{TE}} e^{-2Q_2 H_2} + \Delta_{m1}^{\text{TE}} \Delta_{2m}^{\text{TE}} e^{-2(Q_1 H_1 + Q_2 H_2)} + \Delta_{2m}^{\text{TE}} e^{-2(Q_1 H_1 + Q_m b)} + \Delta_{m1}^{\text{TE}} e^{-2(Q_2 H_2 + Q_m b)} \\
&\quad + e^{-2(Q_1 H_1 + Q_2 H_2 + Q_m b)}, \\
\mathcal{I}_{mn}^{\text{TM}} &= -\Delta_{2n}^{\text{TM}} e^{-2Q_2 H_2} - \Delta_{nm}^{\text{TM}} e^{-2(Q_n a + Q_2 H_2)} - \Delta_{m1}^{\text{TM}} e^{-2Q_1 H_1} + \Delta_{2n}^{\text{TM}} \Delta_{m1}^{\text{TM}} e^{-2(Q_1 H_1 + Q_2 H_2)} \\
&\quad - \Delta_{2n}^{\text{TM}} \Delta_{nm}^{\text{TM}} \Delta_{m1}^{\text{TM}} e^{-2(Q_n a + Q_1 H_1)} + \Delta_{nm}^{\text{TM}} \Delta_{m1}^{\text{TM}} e^{-2(Q_1 H_1 + Q_2 H_2 + Q_n a)} - \Delta_{nm}^{\text{TM}} e^{-2(Q_m b + Q_1 H_1)} \\
&\quad - \Delta_{2n}^{\text{TM}} \Delta_{nm}^{\text{TM}} \Delta_{m1}^{\text{TM}} e^{-2(Q_m b + Q_2 H_2)} + \Delta_{2n}^{\text{TM}} \Delta_{nm}^{\text{TM}} e^{-2(Q_1 H_1 + Q_2 H_2 + Q_m b)} - \Delta_{2n}^{\text{TM}} e^{-2(Q_n a + Q_m b + Q_1 H_1)} \\
&\quad - \Delta_{m1}^{\text{TM}} e^{-2(Q_n a + Q_m b + Q_2 H_2)} + e^{-2(Q_1 H_1 + Q_2 H_2 + Q_n a + Q_m b)}, \\
\mathcal{J}_{mn}^{\text{TM(TE)}} &= 1 + \Delta_{2n}^{\text{TM(TE)}} \Delta_{nm}^{\text{TM(TE)}} e^{-2Q_n a} + \Delta_{m1}^{\text{TM(TE)}} \Delta_{nm}^{\text{TM(TE)}} e^{-2Q_m b} + \Delta_{2n}^{\text{TM(TE)}} \Delta_{m1}^{\text{TM(TE)}} e^{-2(Q_n a + Q_m b)}, \\
\mathcal{I}_{mn}^{\text{TE}} &= +\Delta_{2n}^{\text{TE}} e^{-2Q_2 H_2} + \Delta_{nm}^{\text{TE}} e^{-2(Q_n a + Q_2 H_2)} + \Delta_{m1}^{\text{TE}} e^{-2Q_1 H_1} + \Delta_{2n}^{\text{TE}} \Delta_{m1}^{\text{TE}} e^{-2(Q_1 H_1 + Q_2 H_2)} \\
&\quad + \Delta_{2n}^{\text{TE}} \Delta_{nm}^{\text{TE}} \Delta_{m1}^{\text{TE}} e^{-2(Q_n a + Q_1 H_1)} + \Delta_{nm}^{\text{TE}} \Delta_{m1}^{\text{TE}} e^{-2(Q_1 H_1 + Q_2 H_2 + Q_n a)} + \Delta_{nm}^{\text{TE}} e^{-2(Q_m b + Q_1 H_1)} \\
&\quad + \Delta_{2n}^{\text{TE}} \Delta_{nm}^{\text{TE}} \Delta_{m1}^{\text{TE}} e^{-2(Q_m b + Q_2 H_2)} + \Delta_{2n}^{\text{TE}} \Delta_{nm}^{\text{TE}} e^{-2(Q_1 H_1 + Q_2 H_2 + Q_m b)} + \Delta_{2n}^{\text{TE}} e^{-2(Q_n a + Q_m b + Q_1 H_1)} \\
&\quad + \Delta_{m1}^{\text{TE}} e^{-2(Q_n a + Q_m b + Q_2 H_2)} + e^{-2(Q_1 H_1 + Q_2 H_2 + Q_n a + Q_m b)}.
\end{aligned} \tag{D1}$$

[1] H. B. G. Casimir, Proc. K. Ned. Akad. Wet. **51**, 793 (1948).

[2] P. W. Milonni, *The Quantum Vacuum* (Academic, San Diego, 1994); P. W. Milonni, R. J. Cook, and M. E. Gog-

- gin Phys. Rev. A **38**, 1621 (1988).
- [3] A. Lambrecht, Phys. World Sept. 29 (2002).
- [4] H. B. Chan, V. A. Aksyuk, R. N. Kleiman, D. J. Bishop, and F. Capasso, Phys. Rev. Lett. **87**, 211801 (2011); Science **291**, 1941 (2001).
- [5] E. Buks and M. L. Roukes, Phys. Rev. B **63**, 033402 (2001); Nature (London) **419**, 119 (2002).
- [6] W. Broer, H. Waalkens, V. B. Svetovoy, J. Knoester and G. Palasantzas, Phys. Rev. Applied **4**, 054016 (2015).
- [7] M. Nasiri, M.F. Miri and R. Golestanian, Appl. Phys. Lett. **100**, 114105 (2012).
- [8] F. Chen, U. Mohideen, G. L. Klimchitskaya, and V. M. Mostepanenko, Phys. Rev. Lett. **88**, 101801 (2002); Phys. Rev. A **66**, 032113 (2002).
- [9] R. Golestanian and M. Kardar, Phys. Rev. A **58**, 1713 (1998);
- [10] T. Emig, A. Hanke, R. Golestanian, and M. Kardar, Phys. Rev. A **67**, 022114 (2003).
- [11] Jalal Sarabadani and MirFaez Miri, Phys. Rev. A **74**, 023801 (2006).
- [12] B. Kiani and J. Sarabadani, Phys. Rev. A **86**, 022516 (2012).
- [13] F. Kheirandish, M. Soltani and J. Sarabadani, Phys. Rev. A **81**, 052110 (2010).
- [14] M. Soltani, J. Sarabadani, F. Kheirandish, and H. Rabhani, Phys. Rev. A **82**, 042512 (2010).
- [15] F. Kheirandish, M. Soltani, and J. Sarabadani, Annals of Physics **326**, 657 (2011).
- [16] J. Sarabadani, M. Soltani, P. Zakeri, and S. A. Jafari, Phys. Rev. A **86**, 022507 (2012).
- [17] H. T. Dung, L. Knöll, and D.-G. Welsch, Optics and Spectroscopy **94**, 829 (2003).
- [18] H. T. Dung, L. Knöll, and D.-G. Welsch, Phys. Rev. A **64**, 013804 (2001).
- [19] L. G. Suttorp, and M. Wubs, Phys. Rev. A **70**, 013816 (2004).
- [20] R. Matloob and H. Falinejad, Phys. Rev. A **64**, 042102 (2001).
- [21] R. Matloob, R. Loudon, M. Artoni, S. M. Barnett, and J. Jeffers, Phys. Rev. A **55**, 1623 (1997).
- [22] A. Sambale, S. Y. Buhmann, H. T. Dung, and D.-G. Welsch, Phys. Rev. A **80**, 051801 (2009) .
- [23] E. Amooghorban, N. A. Mortensen, and M. Wubs, Phys. Rev. Lett. **110**, 153602 (2013).
- [24] C. Raabea, and D.-G. Welsch, Eur. Phys. J. Special Topics **160**, 371 (2008).
- [25] S. Scheel, L. Knöll, T. Opatrný, D.-G. Welsch, Phys. Rev. A **62**, 043803 (2000).
- [26] J. D. Jackson, *Classical Electrodynamics* (Wiley, New York, 1999).
- [27] E. Amooghorban, M. Wubs, N. A. Mortensen, and F. Kheirandish, Phys. Rev. A **83**, 013806 (2011).
- [28] B. Huttner and S. M. Barnett, Eur. Phys. Lett. **18**, 487 (1992).
- [29] L. Ryder, *Quantum Field Theory* (Cambridge University Press, New York, 1996).
- [30] B. Huttner, and S. M. Barnett, Phys. Rev. A **46**, 4306 (1992).
- [31] R. Matloob, and R. Loudon, Phys. Rev. A **53**, 4567 (1996).
- [32] A. A. Zyablovsky, A. V. Dorofeenko, A. P. Vinogradov, and A. A. Pukhov, Photon. Nanostruct.: Fundam. Appl. **9**, 398 (2011).
- [33] R. Podgornik, P. L. Hansen and V. A. Parsegian, J. Chem. Phys. **119** 1070 (2003).
- [34] R. Podgornik, R. H. French and V. A. Parsegian, J. Chem. Phys. **124** 044709 (2006).
- [35] J. Sarabadani, A. Naji, R. Asgari and R. Podgornik, Phys. Rev. B **84** 155407 (2011).
- [36] T. H. Boyer, Phys. Rev. A **9** 2078 (1974).
- [37] V. Hushwater, Am. J. Phys. **65** 381 (1997).
- [38] J. Sarabadani, B. Ojaghi Dogahe and R. Podgornik, Europhysics Letts. Accepted (2015).
- [39] M. Bordag *et al.*, *Advances in the Casimir Effect* (Oxford University Press, New York, 2009).
- [40] R. B. Rodrigues *et al.*, Phys. Rev. Lett. **96**, 100402 (2006); Phys. Rev. A **75**, 062108 (2007).
- [41] S. Scheel, T. Opatrný, and D.-G. Welsch, Optics and Spectroscopy, **91**, 411(2001).
- [42] M.-P. Groza and M. Ducloy, Eur. Phys. J. D **40**, 434 (2006).
- [43] Jalal Sarabadani and MirFaez Miri, Phys. Rev. A **75**, 055802 (2007).
- [44] Jalal Sarabadani and MirFaez Miri, Phys. Rev. A **84**, 032503 (2011).